Precursor proadrenomedullin influences cardiomyocyte survival and local inflammation related to myocardial infarction

Svenja Hinrichs[a,b], Katharina Scherschel[b,c], Saskia Krüger[a,b], Johannes Tobias Neumann[a,b], Michael Schwarzl[a,b], Isabell Yan[a,b], Svenja Warnke[a], Francisco M. Ojeda[a,b], Tanja Zeller[a,b], Mahir Karakas[a,b], Till Keller[d,e], Christian Meyer[b,c], Stefan Blankenberg[a,b], Dirk Westermann[a,b,1], and Diana Lindner[a,b,1,2]

[a]Clinic for General and Interventional Cardiology, University Heart Center Hamburg, 20246 Hamburg, Germany; [b]Partner Site Hamburg/Kiel/Lübeck, German Center for Cardiovascular Research, 20246 Hamburg, Germany; [c]Clinic for Cardiology–Electrophysiology, University Heart Center Hamburg, 20246 Hamburg, Germany; [d]Division of Cardiology, Department of Medicine III, Goethe University Frankfurt, 60598 Frankfurt, Germany; and [e]Partner Site Frankfurt, German Center for Cardiovascular Research, 60589 Frankfurt, Germany

Edited by Jonathan G. Seidman, Harvard Medical School, Boston, MA, and approved August 7, 2018 (received for review December 14, 2017)

Increased adrenomedullin (ADM) levels are associated with various cardiac diseases such as myocardial infarction (MI). ADM is cleaved off from the full-length precursor protein proadrenomedullin (ProADM) during its posttranslational processing. To date, no biological effect of ProADM is reported, while ADM infusion leads to antiapoptotic effects and improved cardiac function. Using an MI mouse model, we found an induction of ProADM gene as well as protein expression during the early phase of MI. This was accompanied by apoptosis and increasing inflammation, which substantially influence the post-MI remodeling processes. Simulating ischemia in vitro, we demonstrate that ProADM expression was increased in cardiomyocytes and cardiac fibroblasts. Subsequently, we treated ischemic cardiomyocytes with either ProADM or ADM and found that both proteins increased survival. This effect was diminishable by blocking the ADM_1 receptor. To investigate whether ProADM and ADM play a role in the regulation of cardiac inflammation, we analyzed chemokine expression after treatment of cells with both proteins. While ProADM induced an expression of proinflammatory cytokines, thus promoting inflammation, ADM reduced chemokine expression. On leukocytes, both proteins repressed chemokine expression, revealing antiinflammatory effects. However, ProADM but not ADM dampened concurrent activation of leukocytes. Our data show that the full-length precursor ProADM is biologically active by reducing apoptosis to a similar extent as ADM. We further assume that ProADM induces local inflammation in affected cardiac tissue but attenuates exaggerated inflammation, whereas ADM has low impact. Our data suggest that both proteins are beneficial during MI by influencing apoptosis and inflammation.

adrenomedullin | proadrenomedullin | myocardial infarction | ischemia | cardioprotection

Myocardial infarction (MI) remains a leading cause of morbidity and mortality worldwide (1–4). Post-MI long-term mortality is often related to heart failure (5), which is aggravated by cardiac cell death and local inflammatory processes. Interventions aimed at reducing cardiomyocyte loss and ameliorating inflammation are able to decrease infarct size in experimental settings (6–9). First studies showed that the hormone adrenomedullin (ADM) can reduce cardiomyocyte apoptosis in vitro as well as in vivo and improve cardiac function (10–14).

ADM is expressed in a wide range of tissues including the vasculature and the heart (15–17). The biological function of ADM is mediated by transmembrane receptor dimers generated by a G protein-coupled receptor, the calcitonin receptor-like receptor (CALCRL), and a receptor-activity-modifying protein (RAMP). In particular, the dimer CALCRL/RAMP2 is described as ADM_1 receptor, whereas CALCRL and RAMP3 form the ADM_2 receptor (18). ADM is synthesized as a 185-aa precursor protein named preproadrenomedullin. An N-terminal signal peptide directing the secretory pathway is removed, generating the 164-aa prohormone called proadrenomedullin (ProADM). This prohormone can further be cleaved to at least two biologically active peptides, the 52-aa mature ADM and a 20-aa peptide named "proadrenomedullin N-terminal 20 peptide" (PAMP) (16). The remaining part, flanked by the PAMP and ADM sequence, is called "midregional proadrenomedullin" (MR-proADM) and used for biomarker measurements (19). Increased MR-proADM levels have been reported in different cardiac diseases such as cardiac hypertrophy (20) and heart failure (21–24) as well as MI (25–27) and are associated with increased mortality (26, 28, 29). In contrast to the cleavage products PAMP, MR-ProADM, and ADM, little is known about the full-length precursor ProADM and no biological effects are described so far.

In cardiac tissue, ADM is expressed by cardiomyocytes, cardiac fibroblasts, and endothelial cells (30–32). It has already been described that ADM expression is increased in cardiomyocytes exposed to simulated ischemia, suggesting paracrine effects to reduce cardiomyocyte apoptosis (32). Since gene expression of *proAdm* is highly increased during MI, we aimed to investigate the role of the full-length ProADM and truncated mature ADM in

Significance

Myocardial infarction (MI) is one of the leading causes of death worldwide and is characterized by apoptosis and inflammation. While increased adrenomedullin (ADM) levels after MI are associated with disease severity, ADM infusion leads to antiapoptotic effects, suggesting a self-protective mechanism. ADM is cleaved from a full-length precursor protein (ProADM), a putatively inactive prohormone. Our data show that ProADM is biologically active by reducing apoptosis to a similar extent as ADM. In contrast to ADM, ProADM has proinflammatory effects on cardiac fibroblasts but antiinflammatory effects on activated leukocytes. We assume that ProADM induces local inflammation but attenuates exaggerated inflammation. Our data suggest that both proteins are beneficial during MI by regulating inflammation and reducing apoptosis of cardiomyocytes.

Author contributions: S.H., M.S., T.Z., M.K., T.K., C.M., S.B., D.W., and D.L. designed research; S.H., K.S., S.K., M.S., I.Y., S.W., and D.L. performed research; S.H., K.S., S.K., J.T.N., F.M.O., D.W., and D.L. analyzed data; and S.H., S.K., D.W., and D.L. wrote the paper.

The authors declare no conflict of interest.

This article is a PNAS Direct Submission.

[1]D.W. and D.L. contributed equally to this work.

[2]To whom correspondence should be addressed. Email: d.lindner@uke.de.

This article contains supporting information online at www.pnas.org/lookup/suppl/doi:10.1073/pnas.1721635115/-/DCSupplemental.

Published online August 30, 2018.

post-MI healing processes. In the current study we demonstrate that the putatively inactive ProADM is biologically active, influencing apoptosis as well as local inflammatory processes, suggesting a role in cell survival and healing post-MI.

Results

Up-Regulated mRNA and Protein Levels of ProADM During Acute MI in Mice and Humans. MI was induced by permanent ligation of the left anterior descending artery (LAD) in mice. To analyze gene expression, tissue samples of the left ventricle (LV) were collected from noninfarcted remote zone, border zone, and infarct zone at 1, 5, or 28 d after MI. First, we determined *proAdm* gene expression in the collected cardiac tissue. As shown in Fig. 1*A*, gene expression of *proAdm* was highly increased in the infarct zone 1 d after MI (17.1 ± 4.3-fold) compared with healthy cardiac tissue. The border zone (6.5 ± 1.7-fold) and remote zone (2.8 ± 0.7-fold) reflected the increased gene expression of *proAdm* to a lesser extent. Five and 28 d after MI, gene expression of *proAdm* declined almost to basal levels. Utilizing fluorescence tissue staining, we verified that the increased gene expression level of *proAdm* during the acute MI resulted in higher protein expression of ProADM in the infarct zone compared with the remote zone of the LV (Fig. 1*B*). Next, we examined whether increased ProADM gene and protein expression in cardiac tissue led to increased plasma levels in patients following MI. As illustrated in *SI Appendix*, Fig. S1, a cleavage product is released in equimolar concentrations to ADM but revealed higher stability and is therefore suitable for biomarker measurements (33). Therefore, MR-proADM was detected to estimate the ADM protein expression in patients. MR-proADM concentrations were measured on admission in 1,818 patients presenting with suspected MI (*SI Appendix*, Table S1). Patients with the final diagnosis of MI with non-ST-segment elevation ($n = 211$) showed significantly higher MR-proADM levels compared with patients diagnosed with noncardiac chest pain ($n = 899$) (0.69 vs. 0.57 nmol/L) (*SI Appendix*, Fig. S1).

Increased Apoptosis and Inflammation During the Acute Phase After MI. To explore apoptosis, inflammation, and fibrosis within the remote, border, and infarct zone after MI, we performed additional gene expression measurements as shown in *SI Appendix*, Fig. S3. In general, highest alterations of gene expression were observed within the infarct zone. In detail, the expression level of the proapoptotic gene *Bax* was increased during the acute (1 d) and the subacute phase (5 d) and declined to basal levels 28 d after MI. The proinflammatory genes *Ccl2* (121.1 ± 17.2-fold) and *Ccl7* (43.8 ± 3.7-fold) revealed highly elevated gene expression during the acute phase after MI (1 d). This proinflammatory gene expression diminished during the subacute phase (5 d) and reached basal expression levels 28 d after MI, progressing similarly to the gene expression of *proAdm*. Differently from the *proAdm* expression, profibrotic genes reached their maximum during the subacute phase (5 d) and lasted until 28 d after MI. All gene expression data determined from the infarct zone were combined in Fig. 1*C* to compare their suggested progression during the different phases after MI. This clearly demonstrates that *proAdm* and proinflammatory genes reached their maximum during the acute phase of MI, which was further verified by a significant positive correlation ($r = 0.938$) of *proAdm* and *Ccl2* gene expression (Fig. 1*D*). The increased *Ccl2* gene expression led to increased MCP-1 protein expression as visualized by fluorescence microscopy in Fig. 1*B*. ProADM and MCP-1 were detected within the infarct and border zones during the acute phase after MI. This is in line with the increased number of inflammatory cells observed in the H&E-stained cross-sections. Representative cross-sections are shown in Fig. 1*E*. During the acute phase after MI, changes of the affected myocardium are visible in the more detailed images. The infarct zone showed severe structural alterations and cellular disorganization due to invaded inflammatory cells and necrosis/apoptosis 1 d after MI. Subsequently, this resulted in a loss of cardiomyocytes, which is shown in the infarct zone 5 d after MI, in which pink-stained cardiomyocytes are no longer present. Representative photographs of triphenyltetrazoliumchloride (TTC)-stained whole hearts are presented at different time points after MI and tissue injury of the myocardium was visualized (Fig. 1*F*). The LAD ligation led to impaired cardiac function or even death as plotted as survival curve in Fig. 1*G*. The impaired cardiac function is demonstrated by reduced ejection fraction and increased endsystolic volume (V_{es}) and enddiastolic (V_{ed}) volume compared with sham-operated mice as presented in *SI Appendix*, Table S2.

Ischemia Induced ProADM Expression in Cardiac Cells in Vitro. To determine the cellular source of ProADM after MI, we investigated cardiomyocytes and cardiac fibroblasts in individual cell cultures. As shown in Fig. 2*A*, ProADM (green) was counterstained with the myocyte marker troponin T (TnT, magenta), demonstrating ProADM protein expression in cultured cardiomyocytes. This result was confirmed in cardiac tissue sections, revealing colocalization of ProADM and TnT in cardiomyocytes (Fig. 2*A*). In cultured cardiac fibroblasts, ProADM (green) is expressed as well. Furthermore, ProADM was counterstained with the filament marker Vimentin (VIM, magenta) to label cardiac fibroblasts. In cardiac tissue, similar staining revealed colocalization of both proteins shown in white (Fig. 2*A*, indicated by arrows). Thus, cardiomyocytes as well as cardiac fibroblasts were identified as a source of ProADM. To verify these data, we assessed and compared gene expression levels of *proAdm* in cardiac tissue, cardiomyocytes, cardiac fibroblasts, and leukocytes (splenocytes). As shown at the bottom of Fig. 2*B*, under basal conditions the highest gene expression of *proAdm* was detected in cardiac fibroblasts (0.43 ± 0.05-fold to *Cdkn1b*) and significantly different from cardiac tissue. Cardiomyocytes revealed a substantial *proAdm* expression level as well (0.14 ± 0.02-fold to *Cdkn1b*), which was similar to healthy cardiac tissue (0.16 ± 0.01-fold to *Cdkn1b*). However, primary splenocytes, representing a variety of leukocytes, exhibited very low *proAdm* expression (0.02 ± 0.01-fold to *Cdkn1b*). As described above, *proAdm* expression was highly increased in the infarct zone at 1 d after MI (17.1 ± 4.3-fold to sham). To investigate whether this up-regulation in cardiac tissue can be explained by increased expression in cardiomyocytes or cardiac fibroblasts, we cultured both cell types under simulated ischemia (L-glucose instead of D-glucose and 1% oxygen) and performed gene expression analyses. Indeed, *proAdm* expression increased in cardiomyocytes (11.3 ± 0.9-fold to control) and cardiac fibroblasts (5.1 ± 1.3-fold to control) already after 6 h under simulated ischemia, as shown at the top of Fig. 2*B*. Since MI is accompanied by inflammation and fibrosis, cardiomyocytes and cardiac fibroblasts were exposed to the proinflammatory cytokine TNF-α (10 ng/mL) and the profibrotic growth factor TGF-β (5 ng/mL). As shown in *SI Appendix*, Fig. S2*B*, both proteins hardly influence *proAdm* expression levels in cardiomyocytes. In cardiac fibroblasts, however, proinflammatory stimulation with TNF-α resulted in extensively increased *proAdm* expression (12.1 ± 3.1-fold to control), whereas the profibrotic and antiinflammatory stimulation using TGF-β dramatically decreased the expression (−11.0 ± 0.1-fold to control). Furthermore, to prove whether increased *proAdm* expression during acute MI is caused by infiltrating inflammatory cells into the myocardium, we used primary splenocytes. As shown in Fig. 2*B*, these cells were activated using phorbol-12-myristat-13-acetate (PMA, 100 ng/mL), resulting in a moderate increase of *proAdm* expression (2.9 ± 0.2-fold to control). Since we described cardiac cells as one source of ProADM within cardiac tissue, we were interested whether the precursor protein ProADM or the posttranslationally cleaved ADM is secreted into the extracellular space. Therefore, we used a specific

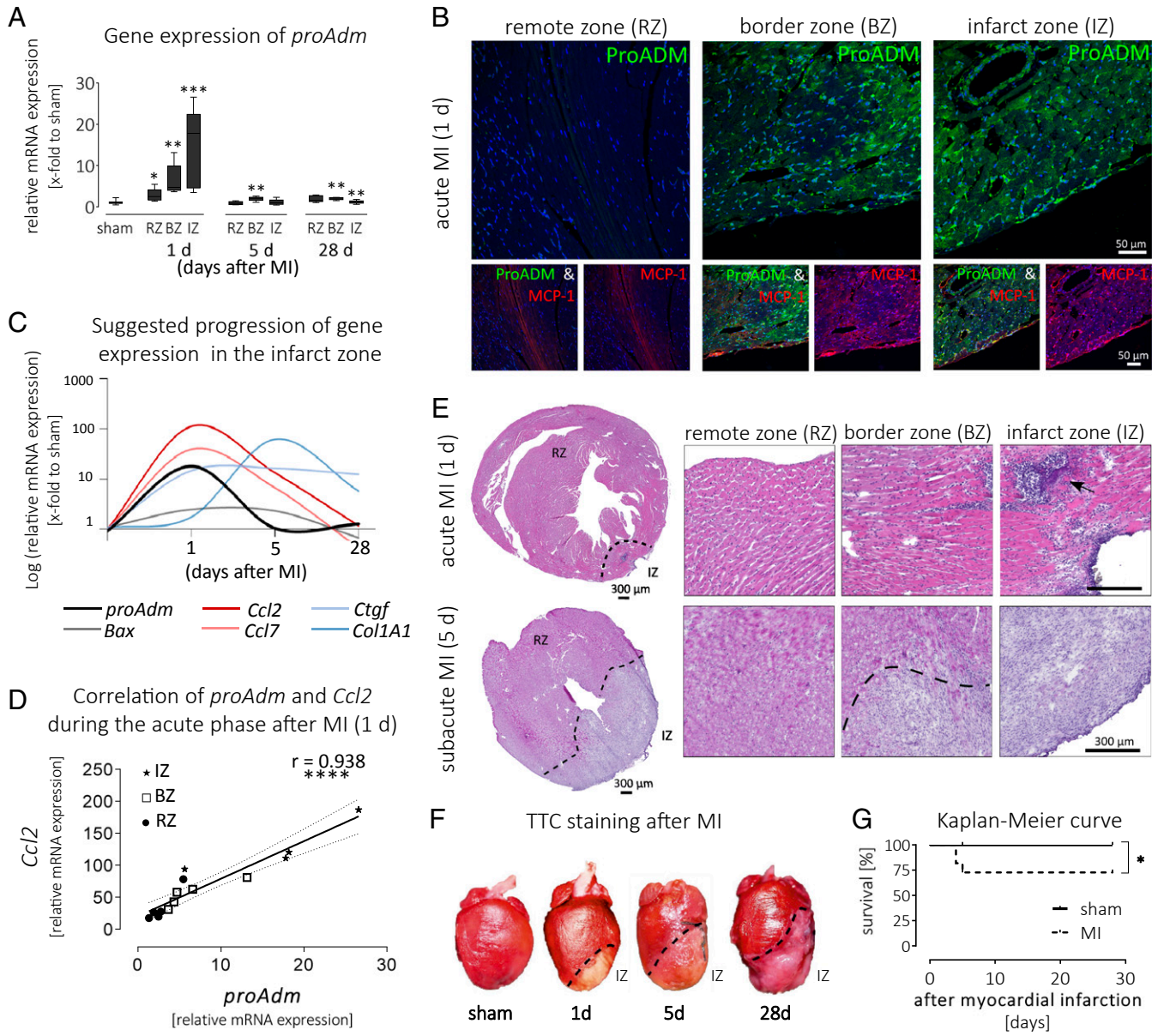

Fig. 1. ProADM is up-regulated during acute MI in mice. (*A*) MI was induced by permanent ligation of the LAD in mice. Gene expression of *proAdm* was analyzed in the remote zone (RZ), border zone (BZ), and infarct zone (IZ) of the LV 1, 5, or 28 d after MI and plotted as x-fold to LV tissue from sham-operated mice. During acute MI, gene expression of *proAdm* was highly increased in the infarct zone and revealed milder gene expression in the border and remote zone. After 5 and 28 d, the *proAdm* gene expression declined almost to basal level. (*B*) Immunofluorescent staining of ProADM (green) and MCP-1 (red) is shown in a representative cross-section of a murine heart 1 d after MI and revealed up-regulated protein expression in the infarct zone and border zone, whereas no ProADM protein expression and low MCP-1 protein expression were determined in the remote zone. (*C*) Summarized gene expression data from the infarct zone are depicted as logarithmized values (detailed data are plotted in *SI Appendix*, Fig. S3) to compare their suggested progression after MI. Similar to *proAdm*, gene expression levels of apoptotic and inflammatory genes reached their maximum after 1 d, whereas the expression of fibrotic genes reached the maximum within the subacute phase (5 d) after MI. (*D*) Analyzing the acute MI, the gene expression of *proAdm* was plotted against the gene expression of *Ccl2* using the data from remote zone, border zone, and infarct zone. A significant positive correlation was found for *proAdm* and the proinflammatory *Ccl2* gene expression ($r = 0.938$). (*E*) Representative H&E-stained cross-sections of murine hearts 1 and 5 d after MI are shown. Histological changes in the infarct zone versus border or remote zones are demonstrated at higher magnification. In the infarct zone, structural alteration and cellular disorganization occurred due to necrosis and apoptosis of cardiomyocytes. Furthermore, inflammatory lesions are present 1 d after MI (indicated by arrow). (*F*) To visualize tissue injury, murine hearts were stained using TTC. Representative photographs from hearts explanted from sham-operated mice or after MI (1, 5, and 28 d) are shown. Red staining represents living tissue, and the infarct zone remains white. (*G*) Survival rate of mice after MI is plotted as Kaplan–Meier curve. Predominantly, mice died during the subacute phase after MI. Gene expression is calculated as relative mRNA expression (x-fold to sham-operated mice) using the formula $2^{-\Delta\Delta Ct}$ and plotted as box plots (minimum to maximum). Gene expression data represent 5–12 mice per time point. Significantly different compared with sham: $*P < 0.05$; $**P < 0.01$; $***P < 0.001$; $****P < 0.0001$. (Scale bar: 300 µm in the H&E-stained cross-sections and 50 µm in the immunofluorescence staining.)

antibody raised against ProADM to investigate cell culture supernatant of cardiac fibroblasts. As positive control, cardiac tissue lysate was used. As shown in Fig. 2*C*, ProADM was detectable within the secretome of cardiac fibroblasts using Western blot analysis, revealing the secretion of ProADM into the extracellular space.

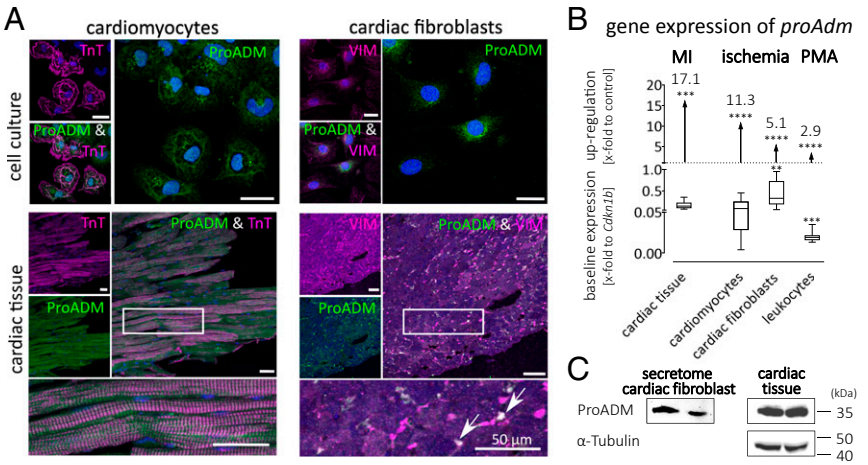

Fig. 2. ProADM expressed in cardiomyocytes and cardiac fibroblasts is up-regulated due to ischemia. (*A*) ProADM (green) was stained in cultured cardiomyocytes and cardiac fibroblasts and revealed vesicular subcellular structures common for secreted proteins. As cell-type–specific markers, cardiomyocyte-specific TnT or fibroblast-specific VIM were used and are visualized in magenta. Both cell types, cardiomyocytes as well as cardiac fibroblasts, express the protein ProADM (green). This was confirmed in cardiac tissue: colocalization of ProADM and the respective cell-specific marker yield in white, which is indicated by arrows at higher magnification. (*B*) Gene expression of *proAdm* was measured in cardiac tissue and individual cell culture samples. At the bottom, basal gene expression of *proAdm* is shown and the highest expression was determined in cardiac fibroblasts. Above, the relative expression of *proAdm* is plotted. The *proAdm* expression is increased due to MI in cardiac tissue (17.1 ± 4.3-fold) or simulated ischemia for 6 h in cardiomyocytes (11.3 ± 0.9-fold) and cardiac fibroblasts (5.1 ± 1.3-fold). Additionally, leukocytes increased *proAdm* gene expression (2.9 ± 0.2-fold) 24 h after activation using PMA. (*C*) The analysis of ProADM protein expression in cardiac tissue and in cell culture supernatant of cardiac fibroblasts revealed that ProADM is secreted. Shown are Western blot analyses of ProADM in cardiac tissue lysate and in the secretome of cardiac fibroblasts. Basal gene expression levels are shown as absolute mRNA expression (x-fold to housekeeping gene *Cdkn1b*) using the formula $2^{-\Delta Ct}$ and presented in box plots (minimum to maximum). Alteration of gene expression is depicted as relative mRNA expression (x-fold to control cells) using the formula $2^{-\Delta\Delta Ct}$. Gene expression data represent three to four independent experiments, each performed in five replicates. Significantly different compared with cardiac tissue: ***$P < 0.001$; ****$P < 0.0001$. (Scale bars: 50 µm.)

ProADM and ADM Revealed Antiapoptotic Effects on Cardiomyocytes Under Ischemic Conditions. As shown in Fig. 1*E*, loss of cardiomyocytes occurred during MI due to necrosis and apoptosis. To interfere in cardiomyocyte apoptosis, we exposed cultured cardiomyocytes to simulated ischemia and treated them either with ProADM (20 nM) or ADM (20 nM) for 24 h. First, we examined cell viability to determine the survival rate of cardiomyocytes under ischemic conditions with or without the additional treatment. As shown in Fig. 3*A*, the viability of cardiomyocytes was significantly decreased to 46% ± 2.7 under ischemic conditions compared with control cells. Treatment of ischemic cardiomyocytes with either ProADM (73% ± 1.9) or ADM (78% ± 2.5) led to significantly increased cell viability. To determine apoptosis, we measured the apoptosis-associated caspase activity as well as the gene expression of the proapoptotic *Bax* and the antiapoptotic *Bcl-2*. The activity of caspase 3/7 was significantly increased due to ischemia (161% ± 3.9) compared with control cells. This increased activity was attenuated by ProADM (132% ± 2.5) or ADM (130% ± 3.5) treatment. Furthermore, we determined the gene expression of *Bax* and *Bcl-2* and plotted the ratio (Fig. 3*A*). This measurement revealed similar results: *Bax*/*Bcl-2* ratio was increased in cardiomyocytes under ischemic conditions and decreased by ProADM and ADM treatment. The observed effects of ProADM might be caused by ProADM itself or by ADM, which is generated by proteolytic cleavage of ProADM, as illustrated in Fig. 3*B*. To clarify the effect of ProADM, we performed similar experiments in the presence of protease inhibitors to avoid ADM formation. As shown in Fig. 3*C*, the antiapoptotic effects of ProADM were still detectable in the presence of protease inhibitor, indicating that ProADM itself is a functional protein. To determine the half-life of ProADM, we used cell culture supernatant from cardiac fibroblasts comprising a variety of proteases mimicking the local myocardial environment. As shown in Fig. 3*D*, the proteolytic cleavage of ProADM is clarified by reduced protein quantity analyzed by Western blot. Determined protein quantity was plotted against the respective hours. Fitting an exponential decay equation using GraphPad Prism, a half-life of 2.0 ± 0.3 h for ProADM was estimated.

Antiapoptotic Effects of ProADM and ADM on Cardiomyocytes Under Ischemic Conditions Mediated by ADM Receptors. First, we determined whether the single receptor components (*Calcrl*, *Ramp2*, and *Ramp3*), forming the two heterodimeric ADM receptor subtypes, are expressed in the cardiac tissue (*SI Appendix*, Fig. S2*A*) and particularly in cardiomyocytes (Fig. 4 *A* and *B*). The ADM_1 receptor consists of CALCRL and RAMP2, whereas the ADM_2 receptor consists of CALCRL and RAMP3. In the cardiac tissue, all components were expressed and their expression levels were not affected 1 d after MI (*SI Appendix*, Fig. S2*A*), whereas we measured down-regulated gene expression levels in the infarct zone 5 and 28 d after MI. As shown in Fig. 4 *A* and *B*, gene and protein expression data revealed that cardiomyocytes express all components and can thus build both heterodimeric ADM receptor subtypes. As shown in *SI Appendix*, Fig. S2*B*, gene expression of *Calcrl*, *Ramp2*, and *Ramp3* were significantly up-regulated in cardiomyocytes after ischemia for 24 h. To investigate whether ProADM binds to the similar cell surface receptors as ADM, we used the receptor antagonist $ADM_{(22–52)}$ to inhibit the observed antiapoptotic effect of ProADM and ADM using cell viability and caspase assays, as shown in Fig. 4*C*. In our experiments, this receptor antagonist completely blocked the antiapoptotic effect of ProADM and ADM. As published previously, at a ligand concentration of 20 nM ADM, 10 µM of the ADM receptor antagonist $ADM_{(22–52)}$ specifically blocks the ADM_1 but not the ADM_2 receptor subtype (34). Therefore, the antiapoptotic signaling is mediated by the ADM_1 receptor subtype. To investigate the underlying signaling pathways Proteome Profiler Antibody Arrays, designed for the detection of 26 phospho-MAP kinases, were used to screen for candidates. Therefore, we analyzed cell lysates derived from cardiomyocytes under simulated ischemia in the presence or absence of ProADM or ADM as antiapoptotic treatment. In Fig. 4*D*, the results are illustrated as densitometric values and revealed increased phosphorylation of CREB, ERK1/2, and GSK-3α/β caused by simulated ischemia, whereas, additional ProADM or ADM treatment dampened the phosphorylation of ERK1/2. This result was verified by Western blot analyses and revealed indeed significantly increased ERK1/2 phosphorylation induced by ischemia which was prevented to some extent by ProADM and ADM treatment (Fig. 4*E*). To clarify whether the ERK pathway mediates the regulation observed for cell viability and apoptosis of cardiomyocytes under simulated ischemia, we blocked ERK signaling using the specific ERK inhibitor PD98059. This did not result in increased cell viability or decreased apoptosis compared with simulated ischemia without any additional treatment (Fig. 4*F*).

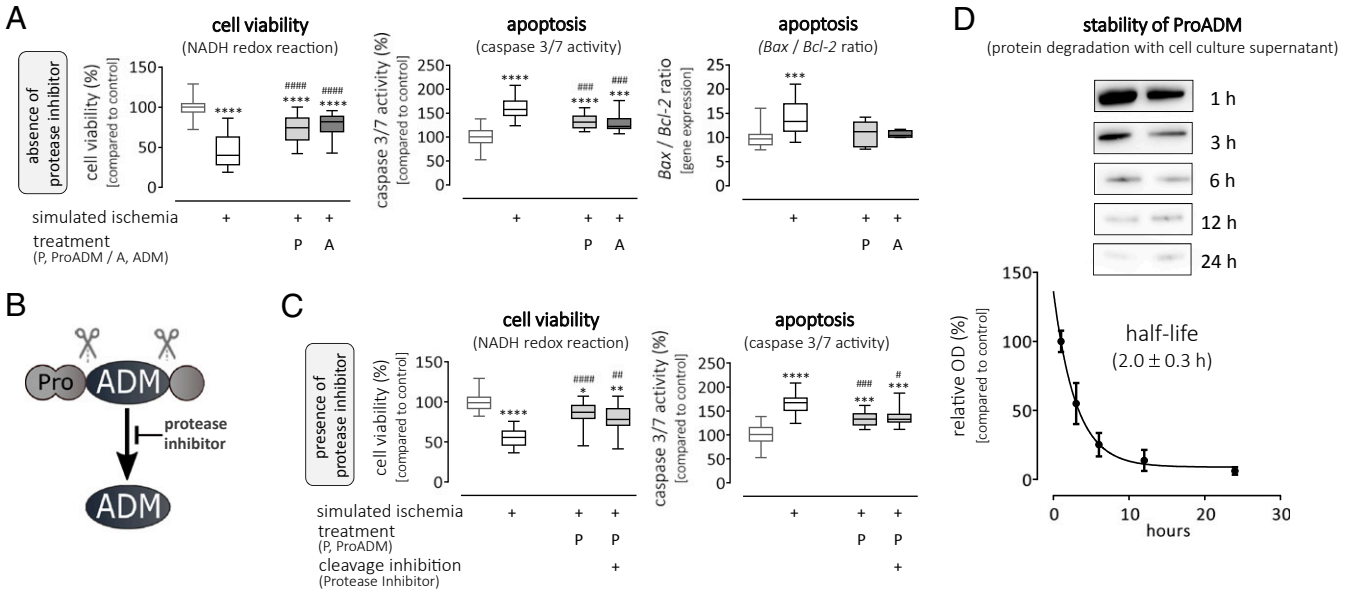

Fig. 3. ProADM and ADM treatment supported cardiomyocyte survival after simulated ischemia in vitro. (*A*) Cardiomyocytes were exposed to simulated ischemia by replacing D-glucose by L-glucose and 1% oxygen for 24 h. Cell viability was reduced due to ischemia but significantly attenuated by ProADM (20 nM) and ADM (20 nM) treatment. Apoptosis-associated caspase 3/7 activity was measured, revealing increased apoptotic activity in cardiomyocytes under ischemic conditions, which could be significantly reduced by ProADM and ADM treatment. Gene expression of *Bax* and *Bcl-2* was measured and plotted as *Bax*/*Bcl-2* ratio. This ratio was significantly increased in cardiomyocytes under ischemic conditions, whereas ProADM and ADM treatment suppressed the elevated apoptotic gene expression. (*B*) ADM is generated from the precursor protein ProADM by posttranslational cleavage, which can be blocked by protease inhibitors. (*C*) In the presence of protease inhibitors, to avoid ADM formation, treatment using ProADM resulted in increased cell viability and reduced caspase 3/7 activity in cardiomyocytes under ischemic conditions for 24 h. (*D*) Stability of ProADM was tested by incubation using cell culture supernatant derived from cardiac fibroblasts. The secretome of cardiac fibroblasts comprised a variety of proteases mimicking the local myocardial environment. Protein quantity was determined by Western blot analysis, plotted against the respective hours. Fitting an exponential decay equation using GraphPad Prism, a half-life of 2.0 ± 0.3 h for ProADM was estimated. Data are presented in box plots (minimum to maximum). Controls are visualized as white bars with gray borders. Data from cardiomyocytes exposed to simulated ischemia are plotted with black borders. Additional treatment is indicated using color-filled bars. Light gray bars represent ProADM treatment, whereas dark gray bars represent ADM treatment. Data represent two to seven independent experiments, each performed in four to eight replicates. Significantly different compared with control cells; $^{*}P < 0.05$; $^{**}P < 0.01$; $^{***}P < 0.001$; $^{****}P < 0.0001$. Significantly different compared with untreated cardiomyocytes under ischemic conditions: $^{\#}P < 0.05$; $^{\#\#}P < 0.01$; $^{\#\#\#}P < 0.001$; $^{\#\#\#\#}P < 0.0001$.

ProADM Revealed Pro- and Antiinflammatory Effects in a Cell-Type-Specific Manner. As described in Fig. 1 *A*–*D*, increased ProADM expression goes along with cardiac inflammation during acute MI. Therefore, we examined the effect of ProADM on two known mediators of cardiac inflammation: cardiac fibroblasts and leukocytes. Each cell type was exposed individually to 20 nM of the full-length precursor protein ProADM for 24 h followed by gene expression analysis. As shown in Fig. 5*A*, ProADM stimulation led to decreased expression of the proinflammatory chemokine *Ccl2* in leukocytes (−1.4 ± 0.08-fold). In contrast, we detected the opposite effect of ProADM stimulation in cardiac fibroblasts with highly upregulated gene expression of *Ccl2* (7.3 ± 0.5-fold) compared with control cells. In contrast, the truncated mature ADM led to antiinflammatory effects on both cell types, which was demonstrated by decreased *Ccl2* expression in leukocytes (−1.3 ± 0.1-fold) and cardiac fibroblasts (−1.5 ± 0.1-fold) compared with control cells (Fig. 5*B*). As shown in *SI Appendix*, Fig. S2*B*, gene expression of *Calcrl*, *Ramp2*, and *Ramp3* was detectable in cardiac fibroblasts, whereas *Ramp2* was not detectable in leukocytes, indicating that cardiac fibroblasts express both ADM receptor subtypes in contrast to leukocytes presenting only the ADM_2 receptor subtype. ProADM and ADM showed opposite functional effects on cardiac fibroblasts, and thus we investigated whether this signal is mediated by the same cell surface receptor as observed on cardiomyocytes. Therefore, we used the receptor antagonist $ADM_{(22–52)}$ to inhibit the observed proinflammatory effect of ProADM and the antiinflammatory effect of ADM on cardiac fibroblasts. Indeed, the effect of ADM was blocked by the receptor antagonist (Fig. 5*B*). Interestingly, the effect of ProADM remained unchanged in the presence of the receptor antagonist $ADM_{(22–52)}$ (Fig. 5*A*), suggesting that ProADM signaling is mediated using a different cell surface receptor. Since both proteins revealed opposite effects, we used mature ADM itself as an antagonist of ProADM on cardiac fibroblasts. Similarly to the truncated $ADM_{(22–52)}$, mature ADM was not able to antagonize the proinflammatory effect of ProADM on cardiac fibroblasts. To strengthen these findings, siRNA knockdown experiments were performed in cardiac fibroblasts. Silencing *Ramp2* expression selectively reduces the expression of the ADM_1 receptor subtype, whereas *Calcrl* silencing abolishes both ADM receptor subtypes. As shown in Fig. 5 *C* and *D*, selective siRNA transfection led to reduced expression levels of *Ramp2* and *Calcrl*, respectively. Subsequent ProADM stimulation did not alter the increase of *Ccl2* expression compared with cardiac fibroblasts without receptor knock-down. ProADM stimulation was not impaired in cardiac fibroblasts lacking either the ADM_1 receptor subtype selectively (Fig. 5*C*) or both subtypes (Fig. 5*D*), which is in line with the finding using the receptor antagonists. To get further insight into the signaling pathway mediated by ProADM in cardiac fibroblasts, we investigated ERK1/2 phosphorylation using Western blot analyses. In contrast to cardiomyocytes, ProADM stimulation induced ERK1/2 phosphorylation in cardiac fibroblasts (*SI Appendix*, Fig. S4*A*). Next, we investigated whether inhibiting the ERK1/2 signaling pathway is sufficient to reduce or block the proinflammatory effect of ProADM in cardiac fibroblasts. Therefore, cardiac fibroblasts were stimulated with ProADM in the presence of the ERK inhibitor PD98059 for 24 h. As depicted in *SI Appendix*, Fig. S4*B*, inhibition of ERK did not dampen the effect of

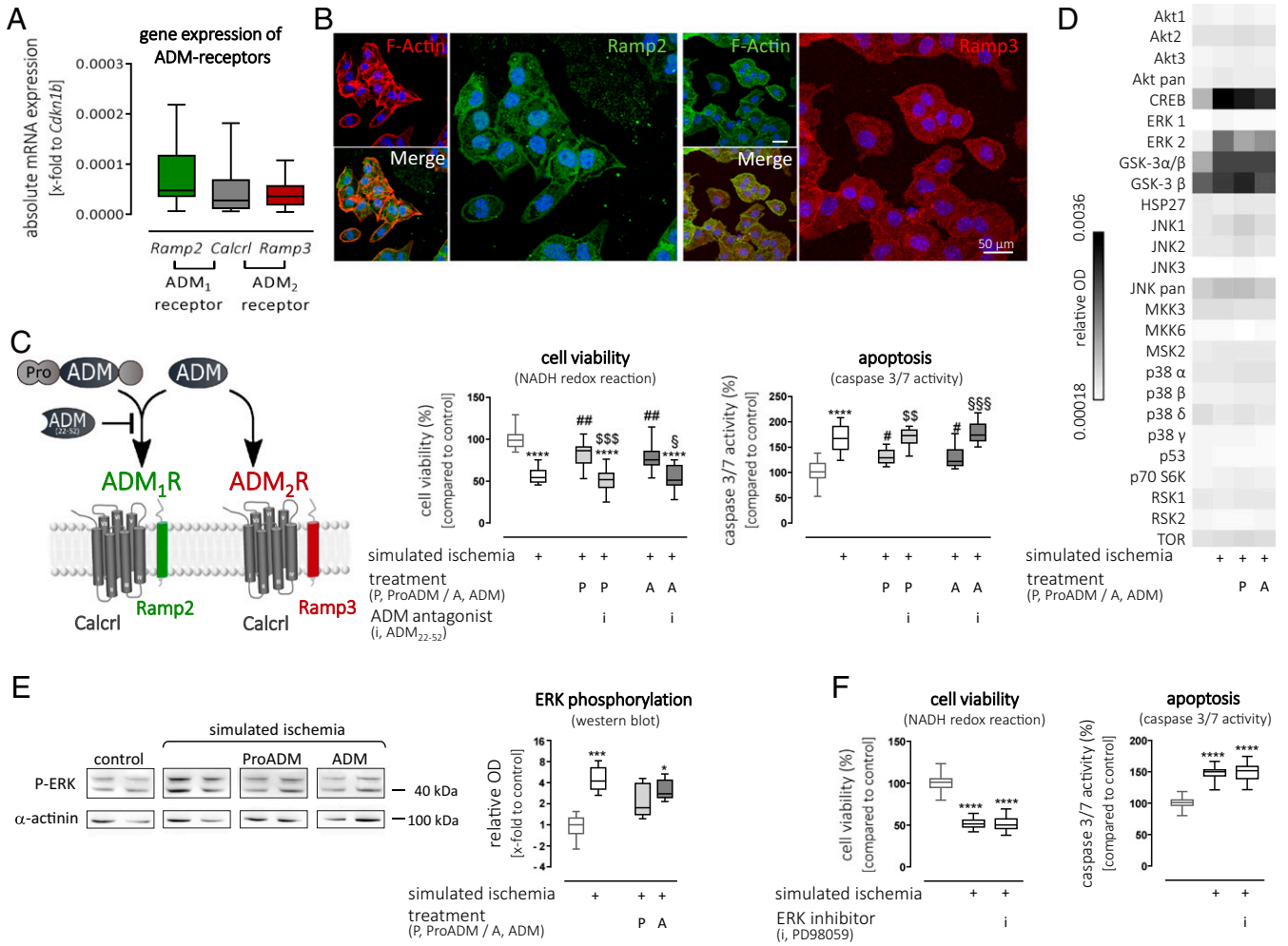

Fig. 4. In cardiomyocytes, antiapoptotic signaling of ADM and ProADM is mediated by ADM_1R subtype. (*A*) Cardiomyocytes revealed gene expression of the single components to assemble the heterodimeric cell surface receptors ADM_1R (*Calcrl* and *Ramp2*) and ADM_2R (*Calcrl* and *Ramp3*). (*B*) Immunofluorescence staining of RAMP2 (green) and RAMP3 (red) in cardiomyocytes confirmed the gene expression data, revealing that both ADM receptor subtypes are present in cardiomyocytes. Cells were counterstained using phalloidin, specific for F-Actin. (*C*) Cell viability and apoptosis were measured in cardiomyocytes after 24 h under simulated ischemia using ProADM or ADM treatment in the presence or absence of the ADM-R antagonist $ADM_{(22–52)}$. It was previously published that at a ligand concentration of 20 nM ADM, 10 μM of the ADM receptor antagonist $ADM_{(22–52)}$ specifically blocks the ADM_1 but not the ADM_2 receptor subtype (34). In the presence of 10 μM $ADM_{(22–52)}$, the antiapoptotic effects of ProADM and ADM were completely blocked, revealing that both proteins use the ADM_1R subtype to mediate the antiapoptotic effects. (*D*) Effects of ADM and ProADM on ischemia-induced phosphorylation of signaling kinases were determined in cardiomyocytes. Before 30 min of simulated ischemia, cardiomyocytes were pretreated 1 h with ProADM or ADM. Cell lysates were applied to Proteome Profiler Antibody Arrays detecting 26 phospho-MAP kinases. Imaged membranes were normalized to the reference spots and averaged signals of duplicated spots are plotted. In general, simulated ischemia induced several signaling pathways in cardiomyocytes by phosphorylation of MAP-kinases, whereas only ERK phosphorylation was prevented by ProADM or ADM treatment to some extent. (*E*) ERK phosphorylation obtained by Proteome Profiler Antibody Arrays was verified utilizing Western blot analyses. Phosphorylation of ERK1/2 under simulated ischemia in the presence or absence of ProADM or ADM treatment was determined in cardiomyocytes. Before 30 min of simulated ischemia, cells were pretreated 1 h with 20 nM ProADM or 20 nM ADM. Cell lysates were analyzed via detection of phosphorylated ERK1/2 using Western blot and two representative lanes are depicted for each subgroup. Quantified ERK phosphorylation was significantly higher after simulated ischemia. ProADM or ADM treatment reduced the ischemia-induced phosphorylation of ERK to some extent. (*F*) Simulated ischemia was applied to cardiomyocytes for 24 h in the presence or absence of 50 μM ERK inhibitor (PD98059). The inhibitor was added 1 h before ischemia. The inhibitor did not repress the reduced cell viability and increased apoptosis due to ischemia. Data are presented in box plots (minimum to maximum). Controls without ischemia are visualized as white bars with gray borders. Data from cardiomyocytes exposed to simulated ischemia are plotted with black borders. Additional treatment is indicated using color-filled bars. Light gray bars represent ProADM treatment, whereas dark gray bars represent ADM treatment. Basal gene expression levels are shown as absolute mRNA expression (x-fold to the housekeeping gene *Cdkn1b*) using the formula $2^{-\Delta Ct}$. Data represent two to seven independent experiments, each performed in four to eight replicates. Significantly different compared with control cells: $^{*}P < 0.05$; $^{***}P < 0.001$; $^{****}P < 0.0001$. Significantly different compared with cardiomyocytes under ischemic conditions: $^{\#}P < 0.05$; $^{\#\#}P < 0.01$. Significantly different compared with cardiomyocytes under ischemic conditions and treated using ProADM: $^{\$\$}P < 0.01$; $^{\$\$\$}P < 0.001$. Significantly different compared with cardiomyocytes under ischemic conditions and treated using ADM: $^{\$}P < 0.05$; $^{\$\$\$}P < 0.001$. (Scale bars: 50 μm.)

ProADM stimulation on the inflammatory gene expression of *Ccl2* in cardiac fibroblasts.

ProADM, but Not ADM, Suppressed Chemokine Expression in Activated Leukocytes. As described in Fig. 5 *A* and *B*, ProADM and ADM stimulation decreased chemokine expression in resting leukocytes. Next, we investigated whether this antiinflammatory effect is still present in activated leukocytes, suggesting that ProADM or ADM treatment can prevent or at least dampen activation. Therefore, we analyzed the alterations of the secretome generated by cardiomyocytes or cardiac fibroblasts under ischemic conditions using Proteome Profiler Antibody Arrays to

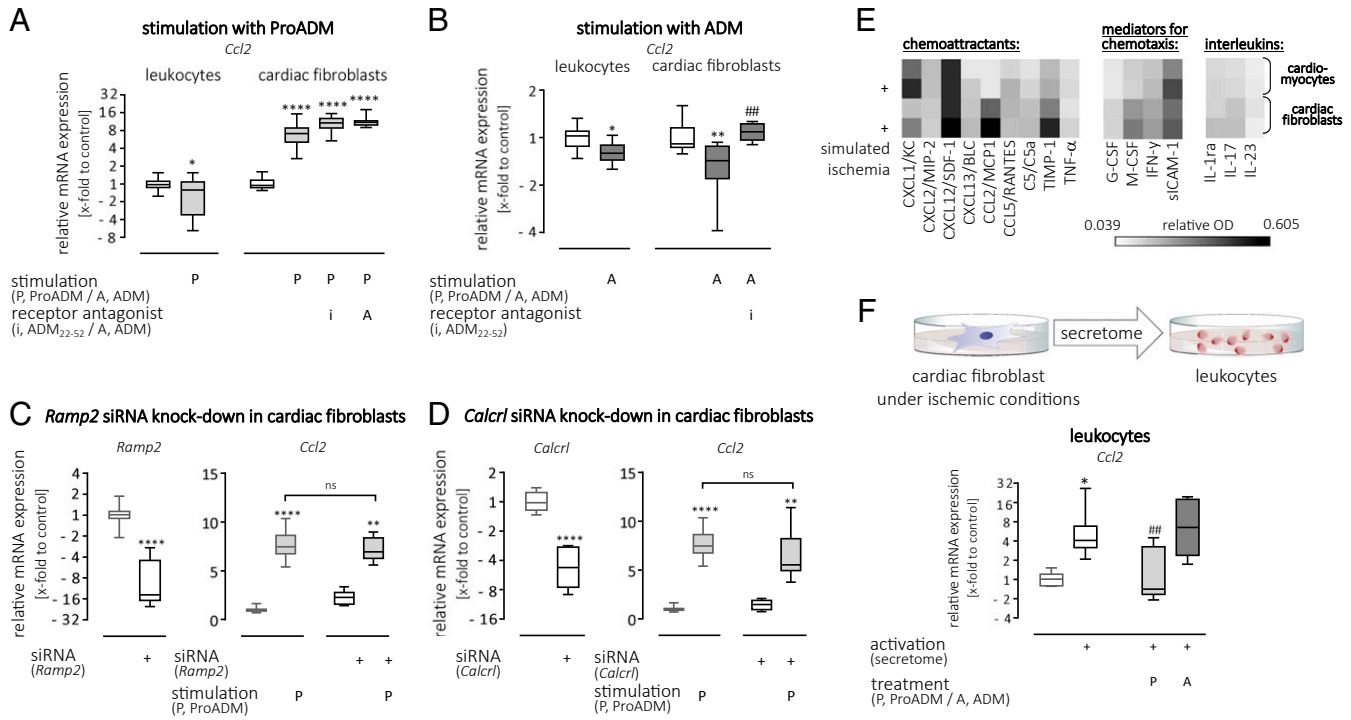

Fig. 5. Inflammatory regulation in cardiac fibroblasts and leukocytes by ProADM and ADM. (*A*) Splenocytes, representing leukocytes, and cardiac fibroblasts were stimulated using 20 nM ProADM for 24 h. Gene expression analysis of the chemokine *Ccl2* revealed antiinflammatory effects on leukocytes but proinflammatory effects on cardiac fibroblasts. This proinflammatory effect on cardiac fibroblasts remained unchanged in the presence of the ADM receptor antagonist $ADM_{(22–52)}$ (10 μM) as well as in the presence of mature ADM itself. (*B*) Splenocytes and cardiac fibroblasts were stimulated with 20 nM ADM for 24 h, which revealed a decreased gene expression of *Ccl2* in both cell types. In cardiac fibroblasts the antiinflammatory effect was blocked in the presence of the ADM receptor antagonist $ADM_{(22–52)}$ (10 μM). (*C*) *Ramp2* expression level was reduced in cardiac fibroblasts 48 h after transfection of siRNA complementary to *Ramp2*. Subsequent ProADM stimulation led to similarly increased *Ccl2* expression in cardiac fibroblasts with or without *Ramp2* silencing. (*D*) *Calcrl* expression level was reduced in cardiac fibroblasts 48 h after transfection of siRNA complementary to *Calcrl*. Subsequent ProADM stimulation induced *Ccl2* expression in cardiac fibroblasts with or without *Calcrl* silencing to the same extent. (*E*) Cytokine secretion from cardiomyocytes and cardiac fibroblasts was detected after 24 h under simulated ischemia. Supernatants from those cells were applied to Proteome Profiler Mouse Cytokine Antibody Arrays. Imaged membranes were normalized to the reference spots and average signals of duplicated spots are plotted. In general, cardiac fibroblasts released chemoattractant molecules or mediators for chemotaxis in a higher range compared with cardiomyocytes which was further induced under ischemic conditions. (*F*) Splenocytes were activated for 24 h using the secretome derived from cardiac fibroblasts cultured under simulated ischemia. Activation of leukocytes led to increased gene expression of *Ccl2*, which could be attenuated by ProADM treatment, whereas treatment using 20 nM ADM did not influence *Ccl2* expression. Data are presented in box plots (minimum to maximum) as relative mRNA expression (x-fold to control cells) using the formula $2^{-\Delta\Delta Ct}$ and represent two to seven independent experiments, each performed in four to eight replicates. Significantly different compared with control cells: $^{*}P < 0.05$; $^{**}P < 0.01$; $^{****}P < 0.0001$. Significantly different compared with activated cells: $^{\#\#}P < 0.01$. ns, not statistically significant.

detect 40 cytokines. The results are illustrated as densitometric values in Fig. 5*E*. In general, cardiac fibroblasts seemed to release chemoattractant molecules or mediators for chemotaxis in a higher range, which were further induced under ischemic conditions. In detail, densitometric analysis revealed increased cytokine expression in cardiac fibroblasts for CCL2 (MCP-1), CXCL12 (SDF-1), TIMP1, CXCL1 (KC), TNF-α, C5/C5a, M-CSF, IL-1ra, IFN-γ, and sICAM-1. In cardiomyocytes CXCL1 (KC), sICAM-1, CCL5 (RANTES), CXCL13 (BLC), TIMP1, C5/C5a, and IFN-γ were increased in the secretome caused by ischemia. To mimic physiological conditions within cardiac tissue during MI, we used the secretome from cardiac fibroblasts generated under ischemic conditions to activate leukocytes. We detected elevated gene expression of the chemokine *Ccl2* (6.9 ± 2.8-fold) as shown in Fig. 5*F*. Next, we used ProADM or ADM as a treatment for activated leukocytes to prove their antiinflammatory effects. Interestingly, ProADM, but not ADM, suppressed the up-regulated gene expression of *Ccl2* of activated leukocytes.

Discussion

The prime finding of the study at hand is that the presumably inactive precursor ProADM is biologically active. As summarized in Fig. 6, it supports cardiomyocyte survival and regulates cardiac inflammation, indicating a role in post-MI remodeling.

ADM: More than a Biomarker. The mature and biologically active hormone ADM is generated by proteolytic cleavage of the full-length precursor protein ProADM. A different cleavage product, MR-proADM, is generated in equimolar concentrations to ADM and is used as a biomarker due to its high stability (33). Increased MR-ProADM plasma levels are reported in patients after acute MI (25) and are predictive for mortality in these patients (26). Here we present that the gene expression of *proAdm* increases after MI in cardiac tissue as well as in cardiomyocytes and cardiac fibroblasts exposed to simulated ischemia. Therefore, elevated plasma levels of MR-proADM might be a result of this increase in *proAdm* gene expression and not necessarily a consequence of necrotic and apoptotic cells. As previously described, it was shown in heterozygous $ADM^{+/-}$ mice that reduced endogenous ADM expression aggravates outcome during cardiac injury (35). However, administration of ADM was able to attenuate LV remodeling and reduce apoptosis of cardiomyocytes after MI or other cardiac damage (10–13). First clinical data were reported that ADM administration after acute MI leads to beneficial hemodynamic effects (36–38), accompanied by a reduction in blood

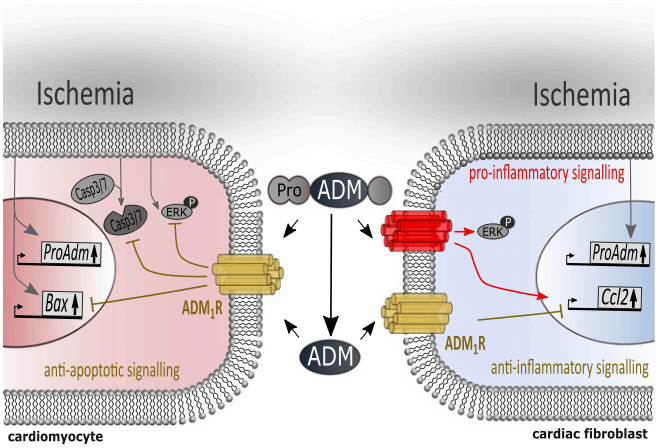

Fig. 6. Schematic overview and summary of presented results. Ischemia induced *proAdm* gene expression in cardiomyocytes and cardiac fibroblasts. This is in line with the finding that increased *proAdm* expression was determined in cardiac tissue during acute MI. Subsequently, ProADM is secreted and posttranslationally cleaved to the truncated mature ADM. Both proteins, ProADM as well as ADM, supported cardiomyocyte survival during simulated ischemia mediated by the ADM_1 receptor subtype. Thus, increased local concentration of both proteins within the ischemic area after MI may be beneficial for cardiomyocytes. In cultured cardiac fibroblasts, the full-length ProADM and the truncated mature ADM revealed counteracting effects. ProADM induced chemokine expression, whereas ADM repressed chemokine expression. The antiinflammatory signaling of ADM is mediated by the ADM_1 receptor subtype, whereas ProADM mediated its proinflammatory effects using signaling receptors different from ADM receptors. Furthermore, ProADM functioned in a cell-specific manner. In cardiomyocytes, ProADM repressed the ischemia-induced ERK phosphorylation. However, in cardiac fibroblasts ProADM stimulation induced ERK phosphorylation.

pressure, which is in line with the reported vasodilatory function of ADM (39). Despite its promising cardioprotective effects, the instability of ADM limits its effectiveness as a potential medical intervention (40). Differently modified ADM analogs have been investigated regarding stability and functionality in vitro (41), to improve its bioavailability. It was already reported that hypoxia induced ADM expression in rat cardiomyocytes but not in cardiac fibroblasts (14). This was also seen in rat hearts post-MI, where ADM immunostaining was limited to myocytes in both the infarcted and noninfarcted regions (42). In our experimental design, we measured the basal expression of *proAdm* and then exposed cardiomyocytes and cardiac fibroblasts to ischemic conditions. In contrast to the current knowledge, both abundant cardiac cell types revealed *proAdm* gene expression. While cardiac fibroblasts exhibited higher basal expression levels compared with cardiomyocytes, ischemic conditions induced *proAdm* gene expression in both cell types. However, leukocytes revealed low basal *proAdm* gene expression, which was slightly increased after activation. Therefore, we suggest that the increased gene expression of *proAdm* after MI is coming from residential cells and might serve as a self-protective mechanism.

Precursor Protein ProADM Improved Cardiomyocyte Survival. Several studies already described antiapoptotic effects of the mature ADM on cardiomyocytes in vitro and in vivo (10–14), but no biological activity has been described for ProADM. In our experiments, we detected the same antiapoptotic effects for ProADM mediated by the ADM_1 receptor. During MI in vivo or simulated ischemia in vitro, cardiac cells increase the expression of ProADM, which may protect cardiomyocytes from entering the apoptotic pathway. Since ischemia induced ERK1/2 phosphorylation, and this phosphorylation was dampened by ProADM as well as ADM treatment, we suggest that the ERK pathway regulates cardiomyocyte survival. However, inhibiting ERK with a commercially available inhibitor was not sufficient to improve cardiomyocyte survival during ischemia. Besides ADM infusion, other cardiac regenerative therapies, such as proregenerative cells or drug administration to the ischemic myocardium, improved cardiac function and have demonstrated potential in preclinical studies (6, 43). Harnessing the endogenous mechanism as potential treatment may have advantages, especially regarding drug safety. However, the reported antiapoptotic effects of ADM during experimental MI were determined using continuous infusion of ADM, which appears to be essential due to the very short half-life of circulating ADM (40). Usually, prohormones are more stable compared with their processed mature hormones. Therefore, unmodified ProADM with a half-life of ∼2 h may provide an alternative to stabilized ADM analogs for antiapoptotic treatment.

Pro- and Antiinflammatory Effects of ProADM and ADM. Besides myocardial cell death, the early phase of the post-MI healing process is further characterized by cardiac inflammation, especially in the ischemic area (44). Interestingly, first data reported regulatory effects of ADM under inflammatory conditions. Infusion of ADM attenuates cardiac inflammation during myocarditis, whereas heterozygous $ADM^{+/-}$ mice revealed higher cytokine response using a murine model of LPS-induced septic shock (45, 46). This genetic modification results in reduced ADM but also ProADM expression levels. Therefore, we investigated both proteins regarding their regulatory ability on cardiac inflammation. Since cardiac fibroblasts are abundantly present within the myocardium and, compared with cardiomyocytes, significantly less sensitive to acute hypoxic conditions induced by MI, they are the first cardiac cells that sense and respond to cardiac injury (47). Following various external stimuli, cardiac fibroblasts increase chemokine expression (48, 49), which we also determined in cardiac fibroblasts exposed to simulated ischemia in the present study. Since these chemoattractant molecules recruit inflammatory cells, cardiac fibroblasts can induce cardiac inflammation. Besides ischemia, cardiac fibroblasts are also exposed to high concentrations of ProADM and ADM during MI. While ProADM induced chemokine expression, ADM stimulation resulted in reduced chemokine expression. Therefore, ProADM stimulates cardiac fibroblasts to induce cardiac inflammation and in turn its cleavage toward mature ADM dampens this proinflammatory effect. In leukocytes ProADM and ADM reduced chemokine expression, suggesting pronounced antiinflammatory effects after established cardiac inflammation. An appropriate inflammatory response is necessary to resolve cardiac damage after acute MI (50), but surrounding healthy heart tissue may be harmed by cardiac inflammation (51). Infiltrated immune cells release cytokines and proteases that induce apoptosis in healthy cardiomyocytes (52). Therefore, anti-inflammatory therapeutics have been considered as a suitable therapy after MI to dampen exacerbated cardiac inflammation (50, 53–58). Since ProADM and ADM stimulation resulted in decreased chemokine expression on quiescent leukocytes, we investigated their antiinflammatory potential on activated leukocytes. Therefore, cells were activated using the secretome of cardiac fibroblasts exposed to ischemic conditions in the presence of ProADM or ADM. ProADM, but not ADM, attenuated further chemokine expression and thus may prevent exaggerated cardiac inflammation.

Receptor Binding of ADM and ProADM. For pharmacological purposes, it is important to identify the binding receptor of ProADM. Since ProADM includes the sequence of ADM, we assumed the same cell surface receptors for both proteins. Two ADM receptors have been described so far: The combination of CALCRL with either RAMP2 or RAMP3 constitutes ADM_1R or ADM_2R, respectively. Concentration response curves revealed EC_{50} values for ADM in low nanomolar ranges for both receptor subtypes (34, 59). Cardiomyocytes express both ADM-R subtypes and a concentration of 20 nM ProADM is sufficient to reveal similar efficacy regarding cardiomyocyte survival as shown for

20 nM ADM. To clarify which ADM receptor subtype mediates the antiapoptotic signaling after ADM and ProADM treatment, we used a receptor-specific antagonist. Truncation of ADM to $ADM_{(22–52)}$ yields an antagonist with higher affinity to ADM_1R. Regarding the structure-affinity studies performed by Robinson et al. (34) and Hay et al. (59), the response to 20 nM ADM mediated by ADM_1R is completely blocked in the presence of 10 μM antagonist, whereas the response mediated by ADM_2R is hardly affected. In our experiments, the antiapoptotic effects of ADM as well as ProADM were blocked in the presence of this antagonist. Therefore, we identified the ADM_1R subtype to bind ADM as well as ProADM and to meditate the antiapoptotic effects on cardiomyocytes. Since cardiac fibroblasts express both ADM-receptor subtypes, we used the ADM_1R antagonist to identify the acting receptor subtype as well. Interestingly, this antagonist inhibited the effect of ADM but not of ProADM, suggesting that ProADM signaling on cardiac fibroblasts is not mediated by ADM_1R. This is in line with the finding that *Ramp2* silencing, which led to selective deficiency of ADM_1R, did not change the ProADM effect. We further investigated whether the proinflammatory signaling of ProADM is mediated by ADM_2R. Since ADM and ProADM revealed opposite effects, ADM may act as a competitive inhibitor on the ADM_2R. Interestingly, ADM was not able to compete against the effects of ProADM, suggesting a receptor different from ADM_1R and ADM_2R. In addition, silencing *Calcrl*, which is essential to form both receptor subtypes, did not alter the ProADM effect on *Ccl2* expression. Furthermore, gene expression data revealed that isolated splenocytes do not express RAMP2 and therefore lack the ADM_1R subtype. Similar antiinflammatory effects for ADM and ProADM were observed in splenocytes. Therefore, we hypothesize that ADM binding to ADM_2R is mediating those antiinflammatory effects. We speculate that ProADM binds to the ADM_2R subtype and thus mediates antiinflammatory effects, but further investigations are required to prove this assumption. So far, we identified the ADM_1R as a ProADM receptor, whereas binding of ProADM to ADM_2R could not be verified. Additionally, we present data on cardiac fibroblasts, in which ProADM binds to a third unknown receptor.

Conclusion. Our findings present biological effects of the full-length precursor protein ProADM. Both proteins, ProADM and the better-characterized truncated form ADM, showed protective and regulatory characteristics regarding post-MI remodeling. Based on our in vitro results, we assume that ProADM induces cardiac inflammation but attenuates established inflammation, while ADM has limited impact on inflammation. However, both proteins improve cardiomyocyte survival under ischemia. This opens up possibilities for ProADM as well as ADM as potential targets to influence postinfarct remodeling.

Materials and Methods

Animals and Surgical Procedures to Induce MI. At the age of 8–12 wk male C57BL/6J (B6) wild-type mice were used to induce MI as described previously (60). The detailed method is described in the *SI Appendix*. All animal experiments were approved by the Hamburg Ministry of Health and Consumer protection, Hamburg, Germany (G15/060) and conform to the *Guide for the Care and Use of Laboratory Animals* (61).

Acute Study Population. Between January 2007 and July 2008, patients with suspected acute coronary syndrome were enrolled in a multicenter study (clinical trial no. NCT03227159 at https://clinicaltrials.gov/) (62). The study was approved by the local ethics committees at Johannes Gutenberg Medical Center, Mainz, Germany and University Hospital Hamburg-Eppendorf, Hamburg, Germany. Participation was voluntary and each patient gave written, informed consent.

Cell Culture. Primary murine cardiac fibroblasts were obtained from the LV tissue of male C57BL/6J wild-type mice (10–12 wk old) as described previously (49) and cultured in DMEM containing 20% FCS, 100 U/mL penicillin, and 100 μg/mL streptomycin (Sigma-Aldrich). The detailed method is described in the *SI Appendix*. The well-established murine cardiomyocyte cell line HL-1 was cultured in Claycomb medium (Sigma-Aldrich) supplemented with 10% FCS, 100 U/mL penicillin, 100 μg/mL streptomycin, 2 mM L-glutamine, and 0.1 μM norepinephrine (Sigma-Aldrich), as recommended (63). Primary murine splenocytes were isolated from freshly removed spleen and immediately used for experiments. The isolation is described in detail in the *SI Appendix*. The distribution of the various leukocytes was determined using FACS analysis. As shown in *SI Appendix*, Fig. S5, the isolated splenocytes consists of 49.7% B cells, 24.5% $CD4^+$ T cells, 14% $CD8^+$ T cells, 0.7% granulocytes, and 0.5% monocytes.

Stimulation and Ischemia in Cell Culture Experiments. Cardiac fibroblasts or cardiomyocytes were starved overnight in DMEM containing 0.5% FCS, 100 U/mL penicillin, and 100 μg/mL streptomycin (Sigma-Aldrich). To simulate ischemic conditions, cells were starved as described above and subsequently exposed to starving medium containing L-glucose instead of D-glucose and placed in a modular incubator chamber (MIC-101; Billups-Rothenberg, Inc.). The chamber was flushed with nitrogen and carbon dioxide using a flow rate ratio of 20 to 1, respectively, until the final oxygen concentration of 1% was reached, detected by an oxygen sensor (Greisinger). ProADM or ADM stimulation was performed using a final concentration of 20 nM recombinant His-tagged murine ProADM (amino acids 24–171) (Cloud-Clone Corp.) or 20 nM synthetic rat ADM (Peptide Institute, Inc.) diluted in starving medium. The recombinant ProADM was tested for endotoxin contamination by Lonza Laboratories (less than 0.05 EU/mL endotoxin in the final experiments). Furthermore, a truncated synthetic human ADM (amino acids 22–52) (Peptide Institute, Inc.) was used in a final concentration of 10 μM. To inhibit proteolytic cleavage, protease inhibitor mixture was used in cell culture experiments in a final dilution of 1 to 1,000 (P8340; Sigma-Aldrich), which did not alter gene expression. To inhibit ERK signaling, cells were treated with 50 μM PD98059 (Sigma-Aldrich) 1 h before stimulation. Cell viability and apoptosis assays were performed as described in *SI Appendix*.

siRNA Knock-Down Experiments. Cardiac fibroblasts were transfected using siRNA complementary to Ramp2 (s79660; Life Technologies) or Calcrl (s79737; Life Technologies). Scrambled siRNA (silencer negative control No.1; Life Technologies) was used as a negative control and showed similar results compared with nontransfected controls. Liptofectamine RNAiMAX reagent (Invitrogen) was incubated with 320 nM of the respective siRNA in OptiMEM (Gibco) for 20 min. Cells were washed once and the prepared lipofectamine/siRNA complex was added. After 30 min, RNA complexes were further diluted to a final concentration of 160 nM siRNA using serum reduced DMEM (Gibco) and exposed to the cells for 24 h. ProADM stimulation was performed 48 h after siRNA transfection as described above.

Gene Expression Analysis. Isolation of total RNA and gene expression analysis are described in *SI Appendix* and gene expression assays are listed in *SI Appendix*, Table S4.

Tissue Staining, Histology, and Immunofluorescence. For histological studies, cross-sections of murine hearts were stained using H&E staining. Furthermore, specific proteins were detected by immunofluorescent staining of cross-sections or cardiac cells as described previously (64). Staining was carried out according to the detailed protocol described in *SI Appendix*.

Proteome Antibody Array and Western Blot. Detection of 40 cytokines or detection of 26 phospho-MAP kinases was performed on Proteome Profiler Antibody Arrays (R&D Systems) according to the manufacturer's instructions using cell culture supernatant or cell lysate, respectively. A more detailed protocol for Proteome Antibody Array and Western blot is described in *SI Appendix*. A list of used antibodies is shown in *SI Appendix*, Table S3.

Statistical Analysis. MR-ProADM levels were analyzed using R version 3.4.2. All other data were analyzed using GraphPad Prism 6 software (GraphPad Software). Statistical comparison of two groups was performed using the Mann–Whitney *U* test. More than two groups were compared using the Kruskal–Wallis test followed by Dunn's posttest. A Grubbs' test was performed to determine significant outliers.

ACKNOWLEDGMENTS. We thank Mareile Schröder and Hartwig Wieboldt for their excellent technical support and the University Hospital Hamburg-Eppendorf Microscopy Imaging Facility (umif), University Hospital Centre Hamburg-Eppendorf for providing microscopes and support as well as the core facility for fluorescence-activated cell sorting at the University Hospital Hamburg-Eppendorf. This work was supported by the German Ministry of Research and Education (German Center for Cardiovascular Research, Grant FKZ 81Z2710107).

1. Thygesen K, Alpert JS, White HD; Joint ESC/ACCF/AHA/WHF Task Force for the Redefinition of Myocardial Infarction (2007) Universal definition of myocardial infarction. *J Am Coll Cardiol* 50:2173–2195.
2. Thygesen K, et al.; Joint ESC/ACCF/AHA/WHF Task Force for Universal Definition of Myocardial Infarction; Authors/Task Force Members Chairpersons; Biomarker Subcommittee; ECG Subcommittee; Imaging Subcommittee; Classification Subcommittee; Intervention Subcommittee; Trials & Registries Subcommittee; Trials & Registries Subcommittee; Trials & Registries Subcommittee; Trials & Registries Subcommittee; ESC Committee for Practice Guidelines (CPG); Document Reviewers (2012) Third universal definition of myocardial infarction. *J Am Coll Cardiol* 60:1581–1598.
3. Reed GW, Rossi JE, Cannon CP (2017) Acute myocardial infarction. *Lancet* 389: 197–210.
4. Nichols M, Townsend N, Scarborough P, Rayner M (2014) Cardiovascular disease in Europe 2014: Epidemiological update. *Eur Heart J* 35:2929.
5. D'Elia N, D'hooge J, Marwick TH (2015) Association between myocardial mechanics and ischemic LV remodeling. *JACC Cardiovasc Imaging* 8:1430–1443.
6. Cleutjens JP, Blankesteijn WM, Daemen MJ, Smits JF (1999) The infarcted myocardium: Simply dead tissue, or a lively target for therapeutic interventions. *Cardiovasc Res* 44:232–241.
7. Boisguerin P, Giorgi JM, Barrère-Lemaire S (2013) CPP-conjugated anti-apoptotic peptides as therapeutic tools of ischemia-reperfusion injuries. *Curr Pharm Des* 19: 2970–2978.
8. Xu T, Li D, Jiang D (2012) Targeting cell signaling and apoptotic pathways by luteolin: Cardioprotective role in rat cardiomyocytes following ischemia/reperfusion. *Nutrients* 4:2008–2019.
9. Yaoita H, Ogawa K, Maehara K, Maruyama Y (1998) Attenuation of ischemia/reperfusion injury in rats by a caspase inhibitor. *Circulation* 97:276–281.
10. Kato K, et al. (2003) Adrenomedullin gene delivery attenuates myocardial infarction and apoptosis after ischemia and reperfusion. *Am J Physiol Heart Circ Physiol* 285: H1506–H1514.
11. Nakamura R, et al. (2004) Adrenomedullin administration immediately after myocardial infarction ameliorates progression of heart failure in rats. *Circulation* 110: 426–431.
12. Okumura H, Nagaya N, Kangawa K (2003) Adrenomedullin infusion during ischemia/reperfusion attenuates left ventricular remodeling and myocardial fibrosis in rats. *Hypertens Res* 26(Suppl):S99–S104.
13. Yoshizawa T, et al. (2016) Effects of adrenomedullin on doxorubicin-induced cardiac damage in mice. *Biol Pharm Bull* 39:737–746.
14. Tokudome T, et al. (2002) Adrenomedullin inhibits doxorubicin-induced cultured rat cardiac myocyte apoptosis via a cAMP-dependent mechanism. *Endocrinology* 143: 3515–3521.
15. Kitamura K, et al. (1993) Adrenomedullin: A novel hypotensive peptide isolated from human pheochromocytoma. *Biochem Biophys Res Commun* 192:553–560.
16. Kitamura K, et al. (1993) Cloning and characterization of cDNA encoding a precursor for human adrenomedullin. *Biochem Biophys Res Commun* 194:720–725.
17. Sakata J, et al. (1993) Molecular cloning and biological activities of rat adrenomedullin, a hypotensive peptide. *Biochem Biophys Res Commun* 195:921–927.
18. McLatchie LM, et al. (1998) RAMPs regulate the transport and ligand specificity of the calcitonin-receptor-like receptor. *Nature* 393:333–339.
19. Morgenthaler NG, Struck J, Alonso C, Bergmann A (2005) Measurement of midregional proadrenomedullin in plasma with an immunoluminometric assay. *Clin Chem* 51:1823–1829.
20. Tsuruda T, et al. (2003) Ventricular adrenomedullin is associated with myocyte hypertrophy in human transplanted heart. *Regul Pept* 112:161–166.
21. Krzeminski K, et al. (2002) Effect of static handgrip on plasma adrenomedullin concentration in patients with heart failure and in healthy subjects. *J Physiol Pharmacol* 53:199–210.
22. Jougasaki M, Wei CM, McKinley LJ, Burnett JC, Jr (1995) Elevation of circulating and ventricular adrenomedullin in human congestive heart failure. *Circulation* 92: 286–289.
23. Kobayashi K, et al. (1996) Increased plasma adrenomedullin levels in chronic congestive heart failure. *Am Heart J* 131:994–998.
24. Nishikimi T, et al. (1995) Increased plasma levels of adrenomedullin in patients with heart failure. *J Am Coll Cardiol* 26:1424–1431.
25. Kobayashi K, et al. (1996) Increased plasma adrenomedullin in acute myocardial infarction. *Am Heart J* 131:676–680.
26. Miyao Y, et al. (1998) Increased plasma adrenomedullin levels in patients with acute myocardial infarction in proportion to the clinical severity. *Heart* 79:39–44.
27. Tzikas S, et al. (2013) MR-proANP and MR-proADM for risk stratification of patients with acute chest pain. *Heart* 99:388–395.
28. Maisel A, et al. (2010) Mid-region pro-hormone markers for diagnosis and prognosis in acute dyspnea: Results from the BACH (Biomarkers in acute heart failure) trial. *J Am Coll Cardiol* 55:2062–2076.
29. Peacock WF (2014) Novel biomarkers in acute heart failure: MR-pro-adrenomedullin. *Clin Chem Lab Med* 52:1433–1435.
30. Isumi Y, et al. (1998) Adrenomedullin production in fibroblasts: Its possible function as a growth regulator of Swiss 3T3 cells. *Endocrinology* 139:2552–2563.
31. Isumi Y, et al. (1998) Regulation of adrenomedullin production in rat endothelial cells. *Endocrinology* 139:838–846.
32. Nguyen SV, Claycomb WC (1999) Hypoxia regulates the expression of the adrenomedullin and HIF-1 genes in cultured HL-1 cardiomyocytes. *Biochem Biophys Res Commun* 265:382–386.
33. Goode KM, Nicholls R, Pellicori P, Clark AL, Cleland JG (2014) The in vitro stability of novel cardiovascular and sepsis biomarkers at ambient temperature. *Clin Chem Lab Med* 52:911–918.
34. Robinson SD, Aitken JF, Bailey RJ, Poyner DR, Hay DL (2009) Novel peptide antagonists of adrenomedullin and calcitonin gene-related peptide receptors: Identification, pharmacological characterization, and interactions with position 74 in receptor activity-modifying protein 1/3. *J Pharmacol Exp Ther* 331:513–521.
35. Niu P, et al. (2004) Protective effects of endogenous adrenomedullin on cardiac hypertrophy, fibrosis, and renal damage. *Circulation* 109:1789–1794.
36. Kataoka Y, et al. (2010) The first clinical pilot study of intravenous adrenomedullin administration in patients with acute myocardial infarction. *J Cardiovasc Pharmacol* 56:413–419.
37. Nagaya N, et al. (2002) Intravenous adrenomedullin in myocardial function and energy metabolism in patients after myocardial infarction. *J Cardiovasc Pharmacol* 39: 754–760.
38. Kato J, Kitamura K (2015) Bench-to-bedside pharmacology of adrenomedullin. *Eur J Pharmacol* 764:140–148.
39. Nuki C, et al. (1993) Vasodilator effect of adrenomedullin and calcitonin gene-related peptide receptors in rat mesenteric vascular beds. *Biochem Biophys Res Commun* 196: 245–251.
40. Meeran K, et al. (1997) Circulating adrenomedullin does not regulate systemic blood pressure but increases plasma prolactin after intravenous infusion in humans: A pharmacokinetic study. *J Clin Endocrinol Metab* 82:95–100.
41. Schönauer R, et al. (2016) Adrenomedullin 2.0: Adjusting key levers for metabolic stability. *J Med Chem* 59:5695–5705.
42. Nagaya N, et al. (2000) Cardiac adrenomedullin gene expression and peptide accumulation after acute myocardial infarction in rats. *Am J Physiol Regul Integr Comp Physiol* 278:R1019–R1026.
43. Hastings CL, et al. (2015) Drug and cell delivery for cardiac regeneration. *Adv Drug Deliv Rev* 84:85–106.
44. Frangogiannis NG (2014) The inflammatory response in myocardial injury, repair, and remodelling. *Nat Rev Cardiol* 11:255–265.
45. Yanagawa B, et al. (2007) Infusion of adrenomedullin improves acute myocarditis via attenuation of myocardial inflammation and edema. *Cardiovasc Res* 76:110–118.
46. Dackor R, Caron K (2007) Mice heterozygous for adrenomedullin exhibit a more extreme inflammatory response to endotoxin-induced septic shock. *Peptides* 28: 2164–2170.
47. Chistiakov DA, Orekhov AN, Bobryshev YV (2016) The role of cardiac fibroblasts in post-myocardial heart tissue repair. *Exp Mol Pathol* 101:231–240.
48. Lindner D, et al. (2014) Cardiac fibroblasts aggravate viral myocarditis: Cell specific coxsackievirus B3 replication. *Mediators Inflamm* 2014:519528.
49. Lindner D, et al. (2014) Cardiac fibroblasts support cardiac inflammation in heart failure. *Basic Res Cardiol* 109:428.
50. Liu G, et al. (2017) Early treatment with resolvin E1 facilitates myocardial recovery from ischaemia in mice. *Br J Pharmacol* 175:1205–1216.
51. Westermann D, et al. (2011) Reduced degradation of the chemokine MCP-3 by matrix metalloproteinase-2 exacerbates myocardial inflammation in experimental viral cardiomyopathy. *Circulation* 124:2082–2093.
52. Pulkki KJ (1997) Cytokines and cardiomyocyte death. *Ann Med* 29:339–343.
53. Cheng B, Chen HC, Chou IW, Tang TW, Hsieh PC (2017) Harnessing the early post-injury inflammatory responses for cardiac regeneration. *J Biomed Sci* 24:7.
54. Iyer RP, et al. (2016) Early matrix metalloproteinase-9 inhibition post-myocardial infarction worsens cardiac dysfunction by delaying inflammation resolution. *J Mol Cell Cardiol* 100:109–117.
55. Wang B, et al. (2017) Myoblast transplantation improves cardiac function after myocardial infarction through attenuating inflammatory responses. *Oncotarget* 8: 68780–68794.
56. Anzai A, et al. (2017) The infarcted myocardium solicits GM-CSF for the detrimental oversupply of inflammatory leukocytes. *J Exp Med* 214:3293–3310.
57. Kleveland O, et al. (2016) Effect of a single dose of the interleukin-6 receptor antagonist tocilizumab on inflammation and troponin T release in patients with non-ST-elevation myocardial infarction: A double-blind, randomized, placebo-controlled phase 2 trial. *Eur Heart J* 37:2406–2413.
58. Morton AC, et al. (2015) The effect of interleukin-1 receptor antagonist therapy on markers of inflammation in non-ST elevation acute coronary syndromes: The MRC-ILA heart study. *Eur Heart J* 36:377–384.
59. Hay DL, et al. (2003) CL/RAMP2 and CL/RAMP3 produce pharmacologically distinct adrenomedullin receptors: A comparison of effects of adrenomedullin22-52, CGRP8-37 and BIBN4096BS. *Br J Pharmacol* 140:477–486.
60. Westermann D, et al. (2008) Biglycan is required for adaptive remodeling after myocardial infarction. *Circulation* 117:1269–1276.
61. National Research Council (2011) *Guide for the Care and Use of Laboratory Animals* (National Academies Press, Washington, DC), 8th Ed.
62. Keller T, et al. (2011) Serial changes in highly sensitive troponin I assay and early diagnosis of myocardial infarction. *JAMA* 306:2684–2693.
63. Claycomb WC, et al. (1998) HL-1 cells: A cardiac muscle cell line that contracts and retains phenotypic characteristics of the adult cardiomyocyte. *Proc Natl Acad Sci USA* 95:2979–2984.
64. Jungen C, et al. (2017) Disruption of cardiac cholinergic neurons enhances susceptibility to ventricular arrhythmias. *Nat Commun* 8:14155.